Scripta Materialia 251 (2024) 116226

Contents lists available at ScienceDirect

Scripta Materialia

journal homepage: www.journals.elsevier.com/scripta-materialia

Tensile behaviors of rolled and annealed 90W7Ni3Fe alloy

Hua-Shen Zheng [a], Yu-Heng Zhang [a], Jun Cheng [b], Wei-Zhong Han [a,*]

[a] Center for Advancing Materials Performance from the Nanoscale, State Key Laboratory for Mechanical Behavior of Materials, Xi'an Jiaotong University, Xi'an 710049, China

[b] Shaanxi Key Laboratory of Biomedical Metal Materials, Northwest Institute for Non-ferrous Metal Research, Xi'an, 710016, China

ARTICLE INFO

Keywords:
Tungsten heavy alloys
Rolling
Annealing
Tensile
Ductility

ABSTRACT

Tungsten heavy alloys (WHAs) with two-phase composite structures display unique mechanical properties. Here, we explore the effects of rolling strain and annealing temperature on tensile behaviors of 90W7Ni3Fe WHAs. Cold rolling followed by low-temperature annealing (<1000 °C) induces an increase in yield strength at the expense of ductility. The ductility of WHAs can only be restored by raising the annealing temperature to 1000 °C. Keep the annealing at 1000 °C while gradually increasing the rolling strain not only improves the strength of WHAs but also maintain a good ductility. Once exceeding a critical rolling strain of 60 %, the yield strength of WHAs increases to 1480 MPa, while result in a substantial decrease in ductility. The evolutions of two-phase composite structures with rolling and annealing induces the alterations of the tensile properties of WHAs. These results provide a reference for designing thermal-mechanical processing recipes for WHAs.

Tungsten heavy alloys (WHAs), or composites, typically containing 78–98 wt % W and a nickel to iron ratio of 7:3, along with a balance of ductile phase metals like Ni, Fe, Cu, Co, Mo, have displayed excellent mechanical properties [1–9]. The two-phase WHAs have high density (16–18 g/cm^3), high strength (1000–1700 MPa), good ductility (10–30 %) and strong X-ray absorption capacity [10–12]. Therefore, it is widely used in aerospace, medical industry, and particularly in weapons as kinetic energy piercing shell cores [8,13–15]. The core experiences significant tensile and compressive stresses during firing to withstand stress spikes upon launch [12,16,17]. As a result, the advancement of WHAs with enhanced mechanical properties consistently garners attention.

Several investigations demonstrate that the mechanical properties of WHAs can be further improved by thermo-mechanical processing [18–24]. The room-temperature tensile strength of a 93W4.9Ni2.1Fe alloy is increased from 960 MPa to 1487 MPa through hot-hydrostatic extrusion and heat treatment [25,26]. The yield strength of a 90W7Ni3Fe alloy is elevated to 1295 MPa by rotary swaging, which is 93 % higher than that of the as-sintered alloy (671 MPa) [27]. Overall, these studies were focused on enhancing tensile strength solely through pre-deformation, highlighting a potential gap in understanding the synergistic impact of both pre-deformation and heat treatment. On the other hand, the deformation processes used in these studies mainly focus on hot rolling, hot-hydrostatic extrusion, and rotary swaging, etc. The effect of cold rolling and annealing treatments on the mechanical properties of WHAs has not been studied in detail. Moreover, studies have indicated that the ultimate tensile strength and ductility of WHAs exhibit variation with the hot rolling strain, initially increasing until reaching 62 %, saturating at 74 %, and subsequently decreasing at 87 %. However, the underlying mechanisms remain unclear [28,29]. Therefore, it is necessary to clarify the combined effects of rolling strain and annealing treatments on the tensile behaviors of WHAs. A comprehensive understanding of the effects of pre-deformation and heat treatment on WHAs will provide valuable guidance for designing an appropriate thermal-mechanical processing protocol.

In this study, we used 90W7Ni3Fe as model material to explore the effect of rolling strain and annealing temperatures on the tensile properties of WHAs. The as-sintered WHAs underwent an initial annealing process followed by rolling to varying strains and subsequent annealing at different temperatures. We found that a 1000 °C annealing treatment was essential to maintain a good ductility for 90W7Ni3Fe alloy in this work. With a gradual increase in the rolling reductions and keep the 1000 °C annealing enabled an increase in strength without lost in ductility up to 50 % rolling strain.

The as-annealed 90W7Ni3Fe alloy was rolled down to 10 % thickness reduction, followed by annealing at 500 °C, 600 °C, 800 °C, and 1000 °C for 1 h, and the series of WHAs are labeled as R10, R10-AN500, R10-AN600, R10-AN800, and R10-AN1000, respectively. Subsequently, we

* Corresponding author.
E-mail address: wzhanxjtu@mail.xjtu.edu.cn (W.-Z. Han).

https://doi.org/10.1016/j.scriptamat.2024.116226
Received 19 March 2024; Received in revised form 19 April 2024; Accepted 7 June 2024
Available online 12 June 2024

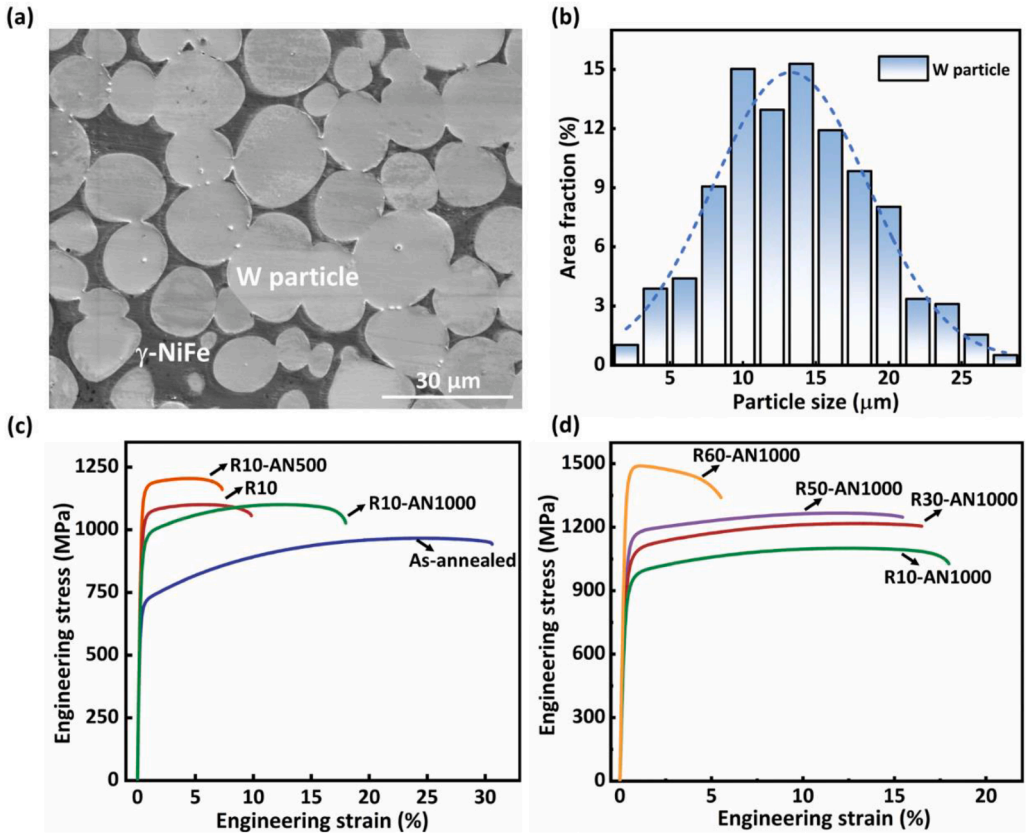

Fig. 1. (a) Initial microstructures and (b) size distribution of W particles in as-annealed WHAs. (c) Engineering stress-strain curves of rolled WHAs with different annealing temperatures. (d) Engineering stress-strain curves of annealed WHAs with different rolling strain.

progressively elevated the rolling strain from 10 % to 60 % and annealed the WHAs at different temperatures after rolling. Tensile samples with dimensions of 15 mm (length) x 4 mm (width) x 2 mm (thickness) underwent room-temperature tensile tests at a strain rate of $1 \times 10–3\ s^{-1}$. Each type of WHAs was repeated for three times. After tensile test, the surface deformation features and fracture surfaces of WHAs were examined using Hitachi SU6600 scanning electron microscope (SEM) and electron backscattered diffraction (EBSD) on a FEI Helios NanoLab dual-beam system.

Fig. 1(a) shows the microstructure of as-annealed WHAs, which consist of near spherical body-centered cubic W particles embedded in face-centered cubic γ-NiFe phase. Fig. 1(b) displays the size distribution of W particles with an average particle diameter of ~15 μm. Fig. 1(c) shows the engineering stress-strain curves of WHAs with different thermal-mechanical treatments. The yield strength of R10 WHAs increase obviously after 10 % rolling strain, while accompanied by a substantial decrease in elongation compared to the as-annealed WHAs. However, the tensile elongation does not recover after annealing at 500 °C, and abnormally a slight increase in yield strength, as shown in Fig. 1 (c). As shown in Fig. S1(a), a similar phenomenon also occurs in WHAs annealed at 600 °C and 800 °C. The increase in strength after low-temperature annealing is likely caused by a decrease of easy glide dislocations in both γ-NiFe phase and W particles [30,31]. When increasing the annealing temperature to 1000 °C, the ductility of rolled and annealed WHAs back to >15 %, accompanied with slight decrease in yield strength, as shown in Fig. 1(c) for R10-AN1000 WHAs. Additionally, the effects of annealing temperature on mechanical properties of WHAs still hold the same trend for 20 % and 30 % rolled samples, as shown in Fig. S1(b) and (c). Furthermore, keep the annealing treatment at 1000 °C can also recover the ductility of WHAs with rolling strain up to 50 %, as shown in Fig. 1(d). In brief, annealing at lower temperatures (<1000 °C) leads to further strengthening, while annealing at 1000 °C could substantially maintain a good elongation. However, once the rolling strain increases to 60 %, the yield strength raises to 1480 MPa, while the elongation drops to 5.5 % even after annealing at 1000 °C. This indicated that there is a critical rolling strain and below which a synergy of strength and ductility can be achieved via thermal-mechanical processing.

Fig. 2 shows the surface morphologies of WHAs after tensile fracture. As shown in Figs. 2(a)–(c), the formation of numerous slip traces in two phases indicate a good deformability of the as-annealed WHAs. In addition, the W-W interparticle fracture and W cleavage microcracks are effectively arrested by the γ-NiFe phase, which consume the strain energy and increase the toughness of the as-annealed WHAs [28,29,32]. For the R10 WHAs, the deformation of W particles is restricted compared to the as-annealed samples since only a few slip traces are produced (Figs. 2(d) and (e)), while the γ-NiFe phase still have very good deformability, as shown by the dense slip traces in Fig. 2(f). After annealing at 500 °C, no evident slip traces were observed in the W particles within R10-AN500 WHAs, and only cleavage fracture occurred in W particles (Figs. 2(g) and (i)). This is related to the recovery of easy glide dislocations in W particles after low temperature annealing, which deteriorate the deformability of W particles and increase the yield strength [22,32]. Once increasing the annealing temperature to 1000 °C, the deformability of W particles is fully recovered, as shown by the intense slip traces formed in W particles (Figs. 2(j) and (l)). Similar deformation characteristics are also observed in R20 series of WHAs (Fig. S2). It is obvious that the modulation of defect structures in two phases by rolling and heat treatment is an effective mean to tune the mechanical properties of WHAs.

EBSD scans were further carried out to reveal the deformation mechanisms of the rolled and annealed WHAs, as shown in Fig. 3. Fig. 3 (a), (d) and (g) show the inverse pole figure (IPF)-Z map of the R10 WHAs after different heat treatments. It can be observed that the shape

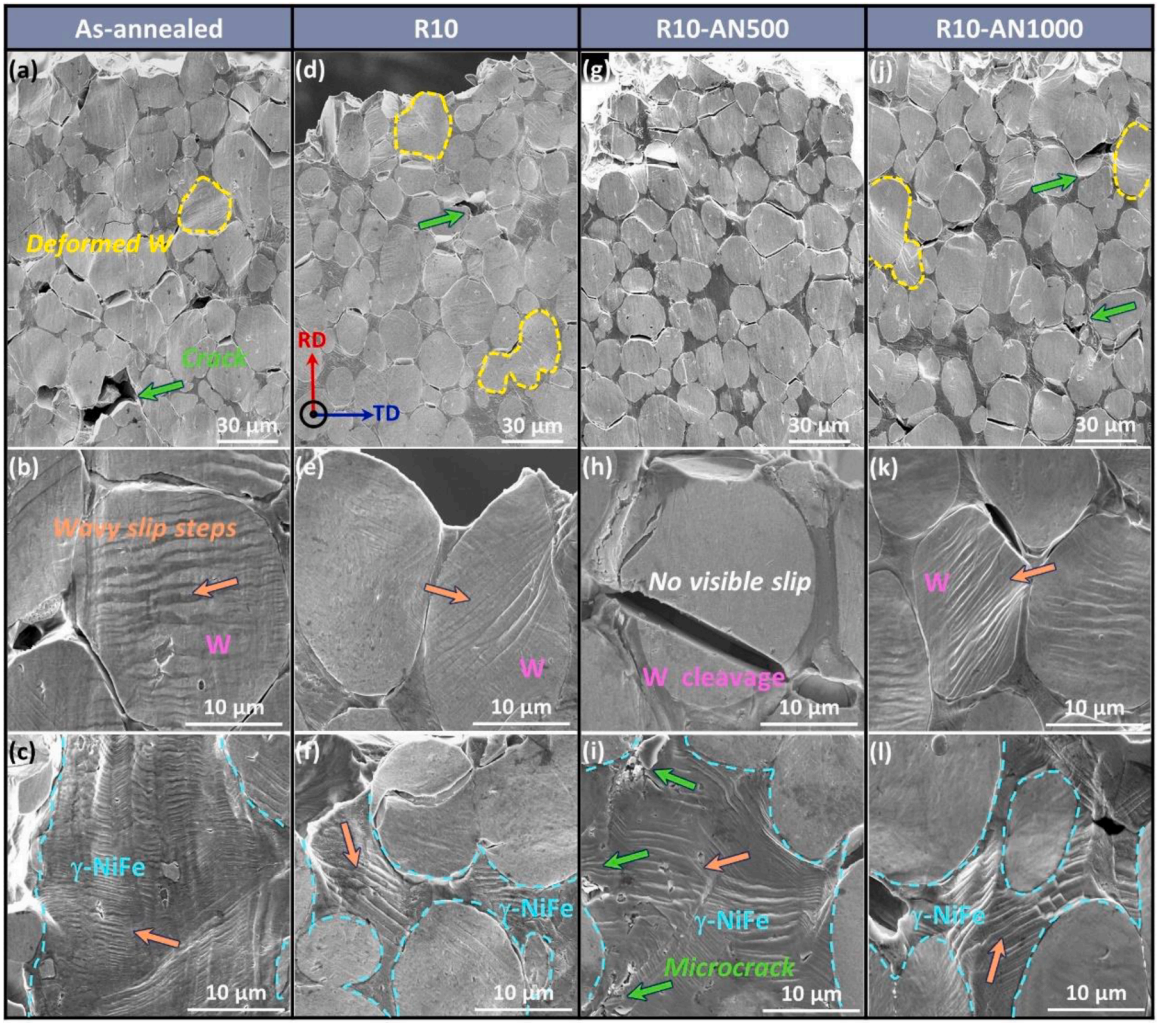

Fig. 2. SEM images showing the surface deformation features of (a-c) as-annealed, (d-f) R10, (g-i) R10-AN500 and (j-l) R10-AN1000 WHAs after tensile fracture. The details of deformed W particles and γ-NiFe phase are enlarged. The green arrows indicate cracks or microcracks, and the orange arrows mark the slip steps in two phases.

and size of W particles are similar in three samples. For R10 WHAs, cold-rolling introduces numerous dislocation structures in two phases, especially in γ-NiFe phase, as highlighted in Fig. 3(b). As a result of dislocation accumulation at the phase boundary, a high interfacial stress triggers dislocations in the W particles, facilitating a coordinated deformation of the γ-NiFe phase and W particles [24,25]. After tensile fracture, numerous sparse dimples are usually formed in γ-NiFe phase in R10 WHAs [26,33], as shown in Fig. 3(c). After annealing at 500 °C, a slightly decrease in dislocation density occurs in both γ-NiFe phase and W particles, as displayed in Fig. 3(e). In particular, low-temperature annealing has a tendency to eliminate all easy glide edge dislocations in W particles, thereby diminishing their deformation capacity [34–38]. Consequently, plastic deformation predominantly occurs in γ-NiFe phase and produce dense dimples, and results in cleavage fracture in W particles, as displayed in Fig. 3(f). Following annealing at 1000 °C, the dislocations in the γ-NiFe phase exhibited significant recovery, accompanied by the formation of some recrystallized small grains, as shown in Fig. 3(g). Moreover, the presence of a smaller fraction of high dislocation density regions in the γ-NiFe phase (as shown in Fig. 3(h)) enables the R10-AN1000 WHAs to maintain a comparable ultimate tensile strength to that of the R10 WHAs. As shown in Fig. 3(i) and Fig. S3(a), the similar fracture morphologies between R10-AN1000 and as-annealed WHAs suggest that the deformability of two phases are largely recovered [35–38]. In a nutshell, 1000 °C post-annealing effectively eliminates the pre-stored dislocation structures within the γ-NiFe phase and immobile screw dislocation in W particles, thereby enhancing the coordinated deformation capacity of two phases.

However, the high-temperature annealing induced recovery of ductility gradually disappeared once the rolling strain increases to 60 %. In particular, the strength of the WHAs increases considerably when the rolling strain is increased from 50 % to 60 %, while the ductility decreases significantly, as shown in Fig. 1(d). The presence of slip traces crossing two phases indicates a good coordinated deformation, and the ductile γ-NiFe phase effectively blunt the cracks in R50-AN1000 WHAs, as shown in Figs. 4(a) and (b). On the contrary, the absence of obvious slip lines in two phases manifest a reduced deformation capacity of R60-AN1000 WHAs, as highlighted in Fig. 4(d). As a result, the cracks cannot be blunted, and extended through the γ-NiFe phase into the adjacent W particles, as shown in Fig. 4(e). To elucidate the diminished deformability of the γ-NiFe phase in the R60-AN1000 sample, a comparative analysis of sample morphologies at varying rolling strains was conducted. The distribution of γ-NiFe phase was observed to become more uniform with increasing rolling strain, accompanied by a gradual decrease in the average thickness between each layer of the long-axis fibrous W particles, as depicted in Fig. S4. This alteration has led to a diminished capacity of the ductile γ-NiFe phase in the R60-AN1000 alloy to accommodate deformation and inhibit crack propagation, as illustrated in Fig. S5. Alterations in the co-deformation capability of the two

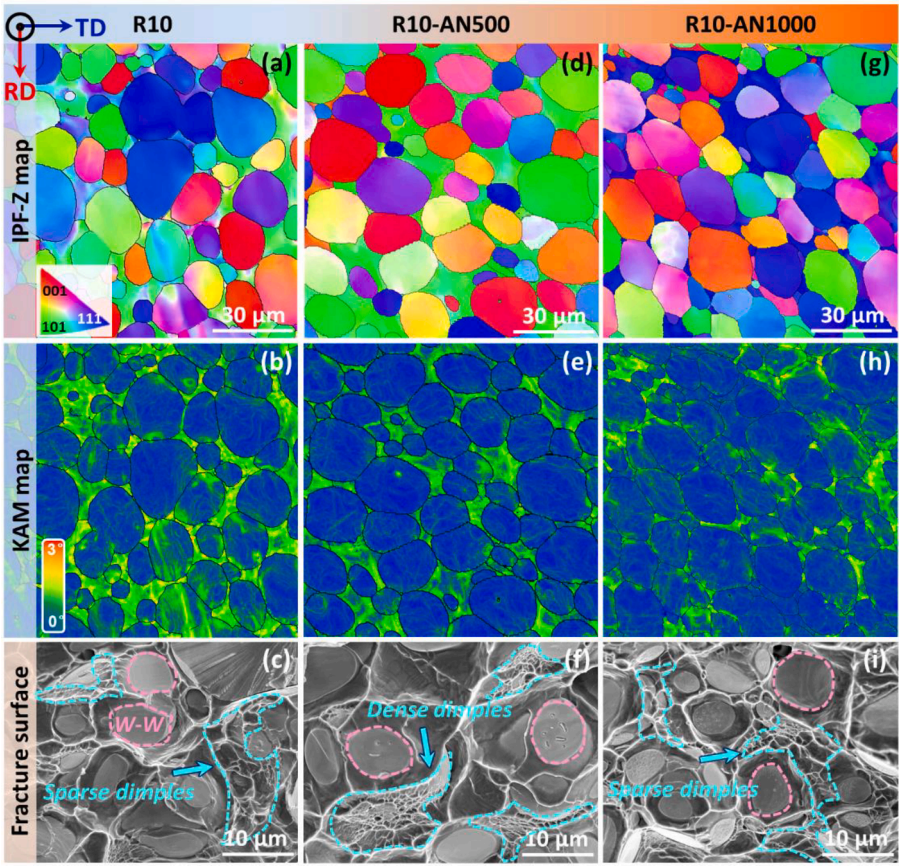

Fig. 3. EBSD scans, KAM maps and tensile fracture morphologies of (a-c) R10, (d-f) R10-AN500 and (g-i) R10-AN1000 WHAs. The KAM is calculated up to the fifth-neighbor shell with a maximum misorientation angle of 3°, which indicate the degree of pre-deformation. The fractured γ-NiFe phases are indicated by the cyan dashed lines and W-W interparticle fracture is indicated by the pink dashed lines.

phases could also induce a shift in the fracture mode of the WHAs. As shown in Fig. 4(g), the proportion of W-W interparticle fracture, which is an unfavorable feature for mechanical performance due to its weaker bonding [6,22,1,39], diminishes as the rolling strain increases from 0 % to 50 %. Meanwhile, the percentage of γ-NiFe phase tearing (γ-γ) gradually increase, which contributes to the enhancement of ductility. In R60-AN1000 alloy, the γ-NiFe phase formed a knife-edge shaped fracture surface (Fig. 4(f)) due to a decrease in average thickness. In contrast, the fracture surface of R50-AN1000 alloy (Fig. 4(c)) still exhibits numerous dimples because of the excellent deformability of the γ-NiFe phase. This is a common phenomenon for WHAs with rolling strain of 20 %−40 % and annealed at 1000 °C, as illustrated in Figs. S3 (b)-(d). Notably, the W particle cleavage (WC) increase with rolling strain, which indicates a gradually harden of the W particles. As a result, the shift in fracture mode of the γ-NiFe phase and the rise in the proportion of W particle cleavage (WC) contribute to a substantial increase in the strength of R60-AN1000 alloy.

Fig. 5 compared the ductility and yield strength of 90W7Ni3Fe WHAs with different combination of rolling and annealing conditions. With increasing rolling strain, a typical strength-ductility tradeoff also appears in the two-phase composite WHAs. Low-temperature annealing (<1000 °C) cannot recover the deformability of WHAs while it alternatively can slightly increase the yield strength, as shown in Fig. 5. Notably, annealing at 1000 °C for 1 h achieves an optimal balance between strength and ductility for the WHAs when the rolled strain is less than 60 %. Upon reaching a rolling strain of 60 %, the yield strength significantly increases, while the tensile elongation decreases to 5.5 %. The thermal-mechanical processing largely alter the initial dislocation structures in two phases thus cause a significant change in their mechanical performance. The evolution of the shape of W particles and the thickness of γ-NiFe phase also play an important role in coordinating deformation of two phases. Once the blunting effect of ductile γ-NiFe phase is completely lost (R60 and R60-AN1000 WHAs), the WHAs only have limited deformability.

In summary, we explore the combination effects of rolling and annealing on the tensile behaviors of WHAs. Annealing at 1000 °C could effectively toughen the rolled WHAs and achieve a balance between strength and ductility, particularly for rolling strain less than 50 %. The evolution of tensile properties of rolled and annealed WHAs is strongly related to the defect structures and the shape of W particles and the thickness of γ-NiFe phase. This study makes contributions to the understanding of deformation behaviors of 90W7Ni3Fe and provides a reference for development high-performance WHAs.

CRediT authorship contribution statement

Hua-Shen Zheng: Writing – original draft, Validation, Methodology, Investigation. **Yu-Heng Zhang:** Writing – review & editing, Validation, Investigation. **Jun Cheng:** Validation, Resources, Investigation. **Wei-Zhong Han:** Writing – review & editing, Writing – original draft, Supervision, Project administration, Investigation, Formal analysis, Conceptualization.

Declaration of interests

The authors declare that they have no known competing financial interests or personal relationships that could have appeared to influence the work reported in this paper.

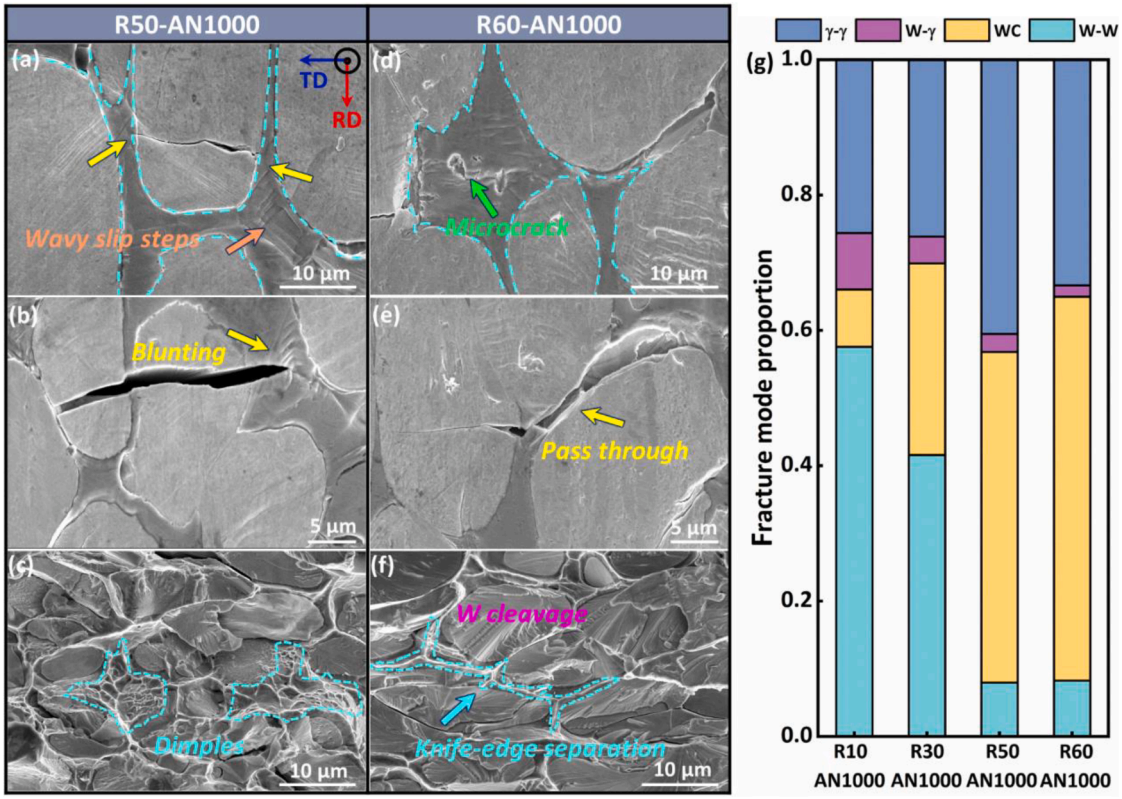

Fig. 4. SEM images showing the deformation and fracture morphologies of (a-c) R50-AN1000 and (d-f) R60-AN1000 WHAs. (g) Statistical ratios of fracture modes in WHAs with different rolling strain, including γ-NiFe phase rupture (γ-γ), W-γ interfacial debonding (W-γ), W cleavage (WC) and W-W interparticle fracture.

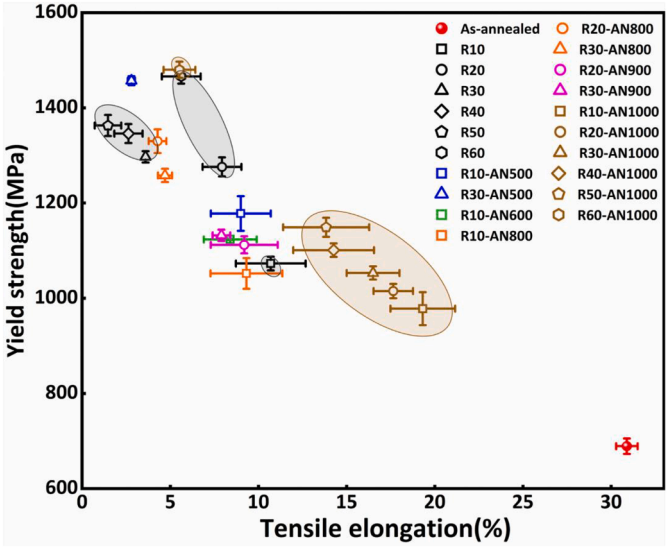

Fig. 5. Summary of tensile properties of WHAs with various rolling strain and annealing conditions.

Acknowledgments

This research was supported by the National Natural Science Foundation of China (Grants Nos. 51971170, 51922082 and 52271249), the Shaanxi Science & Technology Innovation Project (Grant No. 2022QFY10-03) and the Key Research and Development Program of Shaanxi (Grant No. 2023-YBGY-488).

Supplementary materials

Supplementary material associated with this article can be found, in the online version, at doi:10.1016/j.scriptamat.2024.116226.

References

[1] D.V. Edmonds, P.N. Jones, Interfacial embrittlement in liquid-phase sintered tungsten heavy alloys, Metall. Trans. A. 10 (1979) 289–295.
[2] B.C. Muddle, Interphase boundary precipitation in liquid phase sintered W-Ni-Fe and W-Ni-Cu alloys, Metall. Trans. A. 15 (1984) 1089–1098.
[3] R.M. German, L.L. Bourguignon, Analysis of high tungsten content heavy alloys, Powder Metall. Def. Technol. 6 (1984) 117–131.
[4] Z.A. Hamid, S.F. Moustafa, W.M. Daoush, F.A. Mouez, M. Hassan, Fabrication and characterization of tungsten heavy alloys using chemical reduction and mechanical alloying methods, Open J. Appl. Sci. 03 (2013) 15–27.
[5] M. Scapin, Mechanical characterization and modeling of the heavy tungsten alloy IT180, Int. J. Refract. Met. Hard Mater. 50 (2015) 258–268.
[6] X. Gong, J. Fan, F. Ding, Tensile mechanical properties and fracture behavior of tungsten heavy alloys at 25-1100 °C, Mater. Sci. Eng. A. 646 (2015) 315–321.
[7] K. Hu, X. Li, X. Ai, S. Qu, Y. Li, Fabrication, characterization, and mechanical properties of 93W-4.9Ni-2.1Fe/95W-2.8Ni-1.2Fe/95W-2.8Ni-1.2Fe-1Al2O3 heavy alloy composites, Mater. Sci. Eng. A. 636 (2015) 452–458.
[8] M.E. Alam, G.R. Odette, On the remarkable fracture toughness of 90 to 97W-NiFe alloys revealing powerful new ductile phase toughening mechanisms, Acta Mater. 186 (2020) 324–340.
[9] S. Zhou, Y.-J. Liang, Y. Zhu, B. Wang, L. Wang, Y. Xue, Ultrashort-time liquid phase sintering of high-performance fine-grain tungsten heavy alloys by laser additive manufacturing, J. Mater. Sci. Tech. 90 (2021) 30–36.
[10] G. Prabhu, N.A. Kumar, M. Sankaranarayana, T.K. Nandy, Tensile and impact properties of microwave sintered tungsten heavy alloys, Mater. Sci. Eng. A 607 (2014) 63–70.
[11] Y. ŞAHIN, Recent progress in processing of tungsten heavy alloys [J], J. Powder. Technol. 2014 (2014) 764306.
[12] R.M. German, Sintered tungsten heavy alloys: review of microstructure, strength, densification, and distortion, Int. J. Refract. Met. Hard Mater. 108 (2022) 105940.
[13] U. Ravi Kiran, A. Panchal, M. Sankaranarayana, G.V.S. Nageswara Rao, T. K. Nandy, Effect of alloying addition and microstructural parameters on mechanical properties of 93 % tungsten heavy alloys, Mater. Sci. Eng. A 640 (2015) 82–90.

[14] C. Henager, W. Setyawan, T. Roosendaal, N. Overman, B. Borlaug, E. Erickson, K. Wagner, R. Kurtz, G.R. Odette, B. Nguyen, K. Cunningham, Ductile-phase toughened tungsten for plasma-facing materials in fusion reactors, Int. J. Powder Metall. 53 (2017) 53–69.
[15] V.N. Chuvil'deev, A.V. Nokhrin, M.S. Boldin, N.V. Sakharov, G.V. Baranov, V. Y. Belov, A.A. Popov, E.A. Lantsev, E.S. Smirnova, Influence of high-energy ball milling on the solid-phase sintering kinetics of ultrafine-grained heavy tungsten alloy, Dokl. Phys. 62 (2017) 420–424.
[16] H. Couque, G. Nicolas, C. Altmayer, Relation between shear banding and penetration characteristics of conventional tungsten alloys, Int. J. Impact Eng. 34 (2007) 412–423.
[17] A. Kumari, M. Sankaranarayana, T.K. Nandy, On structure property correlation in high strength tungsten heavy alloys, Int. J. Refract. Met. Hard Mater. 67 (2017) 18–31.
[18] J.X. Liu, S.K. Li, X.Q. Zhou, Z.H. Zhang, H.Y. Zheng, Y.C. Wang, Adiabatic shear banding in a tungsten heavy alloy processed by hot-hydrostatic extrusion and hot torsion, Scr. Mater. 59 (2008) 1271–1274.
[19] X.Q. Zhou, S.K. Li, J.X. Liu, Y.C. Wang, X. Wang, Self-sharpening behavior during ballistic impact of the tungsten heavy alloy rod penetrators processed by hot-hydrostatic extrusion and hot torsion, Mater. Sci. Eng. A 527 (2010) 4881–4886.
[20] X. Gong, J.L. Fan, F. Ding, M. Song, B.Y. Huang, J.M. Tian, Microstructure and highly enhanced mechanical properties of fine-grained tungsten heavy alloy after one-pass rapid hot extrusion, Mater. Sci. Eng. A 528 (2011) 3646–3652.
[21] U.R. Kiran, S. Venkat, B. Rishikesh, V.K. Iyer, M. Sankaranarayana, T.K. Nandy, Effect of tungsten content on microstructure and mechanical properties of swaged tungsten heavy alloys, Mater. Sci. Eng. A 582 (2013) 389–396.
[22] Z.S. Levin, K.Ted Hartwig, Hardness and microstructure of tungsten heavy alloy subjected to severe plastic deformation and post-processing heat treatment, Mater. Sci. Eng. A 635 (2015) 94–101.
[23] J.V. Haag, D.J. Edwards, C.H. Henager, W. Setyawan, J. Wang, M. Murayama, Characterization of ductile phase toughening mechanisms in a hot-rolled tungsten heavy alloy, Acta Mater. 204 (2021) 116523.
[24] J. Sun, L. Zhang, Y. Huang, B. Chen, P. Fan, W. Liu, Y. Ma, Effect of rotary swaging on microstructure evolution and adiabatic shear sensitivity of 90W–7Ni–3Fe alloy under dynamic loading, Mater. Sci. Eng. A 860 (2022) 144333.
[25] Y. Yu, L.X. Hu, E.D. Wang, Microstructure and mechanical properties of a hot-hydrostatically extruded 93W-4.9Ni-2.1Fe alloy, Mater. Sci. Eng. A 435 (2006) 620–624.
[26] Y. Yu, W.C. Zhang, E.D. Wang, Effect of heat treatment on microstructure and mechanical properties of hot-hydrostatically extruded 93W-4.9Ni-2.1Fe alloy, J. Alloys Compd. 622 (2015) 880–884.
[27] W.T. Zhu, W.S. Liu, Y.Z. Ma, S.R. Meng, J.N. Wang, Y.T. Duan, Q.S. Cai, Influence of microstructure on crack initiation and propagation behavior in swaged tungsten heavy alloy during Charpy impact process, Mater. Sci. Eng. A. 862 (2023) 144219.
[28] M.E. Alam, J.V. Wang, C.H. Henager, W. Setyawan, G.R. Odette, The effect of hot rolling on the strength and fracture toughness of 90W–7Ni3Fe tungsten heavy metal alloys, Mater. Sci. Eng. A 824 (2021) 141738.
[29] M.E. Alam, J.V. Haag, W. Setyawan, C.H. Henager, G.R. Odette, On the effect of high-temperature annealing on the microstructure and mechanical properties of a hot-rolled 90W7Ni3Fe tungsten heavy alloy, Mater. Sci. Eng. A 896 (2024) 146200.
[30] Y. Lu, Y.H. Zhang, E. Ma, W.Z. Han, Relative mobility of screw versus edge dislocations controls the ductile-to-brittle transition in metals, Proc. Natl. Acad. Sci. USA 118 (2021) e2110596118.
[31] Y. Lu, W.Z. Han, Pre-stored edge dislocations-enabled pseudo-toughness in chromium, Acta Mater. 248 (2023) 118788.
[32] J. Das, G.A. Rao, S.K. Pabi, M. Sankaranarayana, T.K. Nandy, Thermo-mechanical processing, microstructure and tensile properties of a tungsten heavy alloy, Mater. Sci. Eng. A 613 (2014) 48–59.
[33] B.H. Rabin, R.M. German, Microstructure effects on tensile properties of tungsten-nickel-iron composites, Metall. Mater. Trans. A 19 (1988) 1523–1532.
[34] P. Gumbsch, Brittle fracture and the brittle-to-ductile transition of tungsten, J. Nucl. Mater. 323 (2003) 304–312.
[35] R. Gröger, V. Vitek, Multiscale modeling of plastic deformation of molybdenum and tungsten. III. Effects of temperature and plastic strain rate, Acta Mater. 56 (2008) 5426–5439.
[36] B.G. Butler, J.D. Paramore, J.P. Ligda, C. Ren, Z.Z. Fang, S.C. Middlemas, K. J. Hemker, Mechanisms of deformation and ductility in tungsten – A review, Int. J. Refract. Met. Hard Mater. 75 (2018) 248–261.
[37] Y.H. Zhang, W.Z. Han, Mechanism of brittle-to-ductile transition in tungsten under small-punch testing, Acta Mater. 220 (2021) 11732.
[38] Y.-H. Zhang, E. Ma, J. Sun, W.-Z. Han, Unveiling the intrinsic rhenium effect in Tungsten, Acta Mater 264 (2024) 119586.
[39] D.V. Edmonds, Structure/property relationships in sintering heavy alloys, Int. J. Refract. Met. Hard Mater. 10 (1991) 15–26.